

Internal Dosimetry: Combining Simulation with Phantom and *Ex Vivo* Measurement

Bryan J. Stephens, PhD, Wendy Baltzer, DVM, PhD, DACVS, Phil Harrington, DC, CMLSO



INTRODUCTION

Internal dosimetry of laser therapy is far too often overlooked or “guesstimated”, but is crucial information for the design of treatment protocols and prediction of biological efficacy. *In vitro* studies have given us a general idea of the range of biostimulatory doses, but their results do not and should not be directly extrapolated to form conclusions *in vivo*.

The science of dosimetry has been extensively developed in other wavelength ranges of the electromagnetic spectrum to different degrees of precision based on the danger of exposure of each. Though we do not need the sub-millimeter accuracy of the radiation oncologist who delivers ionizing radiation that can destroy individual cells, the techniques they have developed offer a sensible guide to understanding the photon transport in biological tissue. Here we employ some of these tools as we aim to bridge this gap and understand exactly how dose is distributed at depth in the body.

MATERIALS and METHODS

Wavelengths investigated were 800 nm and 970 nm at powers ranging from 0.1 - 12 Watts using the K-1200 (K-LaserUSA, Franklin, TN). First-order predictions were made from power measurements on incremental depths in water and tissue phantoms. Second-order estimates were established by Monte Carlo photon transport simulation on actual MRI data with literature-referenced values of scatter, absorption, and reflection coefficients. Finally, the most robust data came from *ex vivo* Si photodiode detector measurement on six canine cadavers in a variety of anatomical geometries.

2.1 First-Order Approximation

Power meter employed was the PLUS (LaserPoint, Vimodrone, Milano, Italy) using the “LD” calibration setting (quoted by the manufacturer as appropriate for the 800-900 nm range; no significant differences in sensitivity were noted for the 970 nm wavelength).

The meter was placed face-up on a stand to maintain ambient airflow through the heat sink fins. On top was placed a 2 mm thick piece of aluminum with a 1 cm diameter hole punched through that served as an aperture so that spatial independence of the detector head could be verified and radial scattering could be measured. On top of this was placed a thin plastic beaker, whose attenuation was minimal (transmission loss of 2% was measured and all the data corrected accordingly). The laser's handpiece was fixed normal to and at a distance of 12 cm from the beaker/detector interface and irradiation was carried out. In the beaker, layers of water from 0.5 - 10 cm in 0.5 cm increments were added, and the power transmission measured. At each depth of water, the detector was moved relative to the central axis of the beam (laser handpiece position kept constant) to measure transmission values at distances of 0 - 1.5 cm in 0.5 cm increments from the central axis.

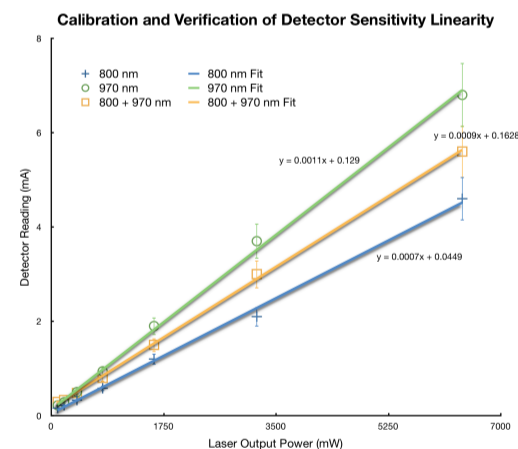


Figure 1: Measurement of Linearity of Response vs Exposed Power for the FDS-1010-CAL for each Wavelength

2.2 Second-Order Approximation

Combining techniques from radiation oncology and neurology, simulations can be performed to give the most detailed prediction of dose deposition. Radiation oncologists pre-plan their irradiations with full 3-dimensional simulations tracking accelerator head motion and collimator leaf manipulation and overlay these parameters on computed tomography images of the patient to ensure highly localized dose distributions. In fact, most linear accelerators on the market come equipped with software capable of performing such estimations, for quality assurance as well as by federal mandate. The interaction of ionizing radiation with biological matter is substantially different from infrared radiation, however, and so the core interactions can not be modeled the same way. Neurologists started using radiation in the near-infrared (NIR) to map the oxygenation of brain tissue since gray- and white- brain matter have distinct signatures in the NIR. To this end, there have been several algorithms developed to track NIR photon transport; used here was the Monte Carlo eXtreme (MCX) [1].

Combining these resources has led to the first Monte-Carlo simulation in laser therapy. The input parameters for the simulation are the absorption coefficient, scattering coefficient, refractive index, and anisotropy factor for each type of tissue. MRI images are used to delineate the exact location of each tissue type and a 7-dimensional matrix (three spatial and 4 parameters) can be formed. Then with enough processing time a computer can initiate a fixed number of photons, originating at any voxel in the matrix, initially traveling in any direction from that origin, and track their transport to every voxel at each time step. Run the simulation for long enough and you have a full laser therapy session modeled and the deposited dose at every voxel recorded.

2.3 Third-Order Approximation

Using a cadaver model and a sensitive photon detector system, a full *ex vivo* dosimetric profile can be established. Resecting various layers of dermis, fat, muscle, and connective tissue, the detector was placed at a variety of depths and the power density delivered to each depth was compared to the surface skin exposure. Normalizing these curves, an accurate model can be formulated to develop pre-planned treatment protocols and quantify the dose dependence of biological effects, post-irradiation. Used were two Si detectors (FDS-100-CAL and FDS-1010-CAL, ThorLabs, Inc., Newton, NJ) whose calibration is NIST traceable, but a power-linearity and wavelength-dependence calibration test was performed on each. Figure 1 shows the measured photocurrent vs exposed power for the full range of experimental values and their fit to a linear model.

Raw Beam Profile: Intensity vs Radial Distance from Central Axis

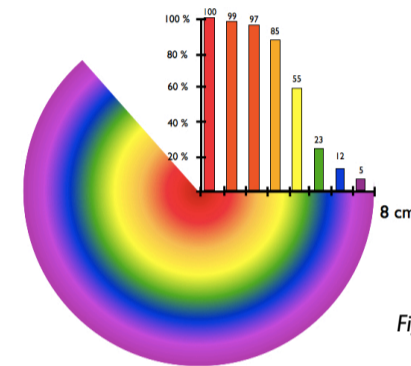


Figure 2: 2-Dimensional Beam Intensity Profile

The same aluminum aperture setup was used to test the spatial sensitivity differences on different parts of the detector wafer, with no significant differences found. This setup was also used to measure the 2-dimensional beam intensity profile, shown in Figure 2 which is clearly not uniform throughout the entire cross-section.

RESULTS

3.1 First-Order Approximation

You can see from the full three-dimensional dose profile in Figure 3 that even in a simple water phantom at the most transparent wavelength (relative to the rest of the NIR) radiation intensity is strongly attenuated with depth. The anisotropy factor at this wavelength in water is about 0.8 which means that 80% of the scattering is directed in the forward hemisphere. This counteracts the absorption losses somewhat, but as you can see the attenuation is still quite steep.

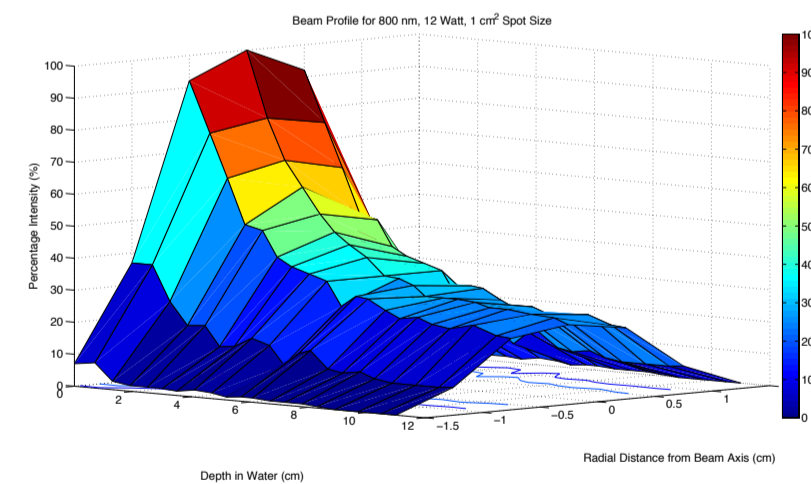


Figure 3: Measured 3-Dimensional Beam Profile in Water Phantom

3.2 Second-Order Approximation

Figure 4 shows the progression of stages in the simulation process. First, the anatomical positions of different tissue types need to be extrapolated from the MRI by a trained radiologist or surgeon. From there, the relevant literature was searched for optical properties of each tissue type at the given wavelength [2-4]. These parameters are overlaid on a contour map extracted from the MRI so that each voxel contains the absorption coefficient, scattering coefficient, anisotropy factor, and refractive index of the corresponding tissue type at the given wavelength. This particular simulation then initiated one billion photons each of which with the initial direction indicated by the red arrow and initial position distributed according to the measured 2-dimensional cross-sectional beam profile measured in Figure 2. The simulation then ran for fifty, 0.1 nanosecond time steps (remember radiation moves at the speed of light and so all the energy gets deposited very quickly) and recorded the absorbed dose in each voxel. Plotted are the values only in the plane of the MRI image, binned in 10% intervals, and normalized to 100% at the surface.

3.3 Third-Order Approximation

Ex vivo measurement is the most accurate, humane form of internal dosimetry estimation. Figure 5 shows the raw data taken on eight canine cadavers of a variety of breeds and in a variety of anatomical arrangements. They are plotted here for simplicity and to show the overall exponential trend in beam attenuation, but this plot does not take into account all of the different types of tissue through which the beam penetrated for each measurement.

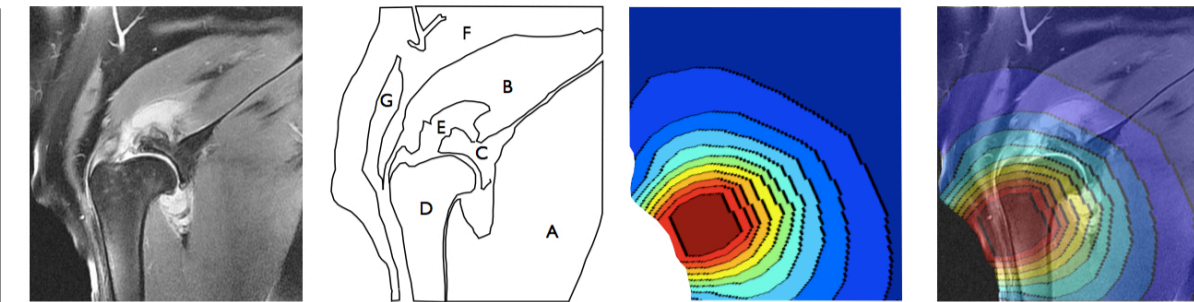


Figure 4: Stages of the Monte-Carlo Dosimetric Simulation. The different tissue types were identified as follows: A - muscle (subscapularis, teres major, latissimus dorsi, triceps) B - muscle (supraspinatus) C - bone (scapula) D - bone (humerus) E - tendon (of the supraspinatus) F - muscle and fat (omotraversarius) G - muscle (deidobranchialis).

As you can see from Figure 4, these measurements included several combinations of skin/hair, fat, muscle, tendons/ligaments, and bone to compile a full dosimetric profile. Also, several beam paths were evaluated to acquire optimal penetration angles.

Example

The depth from the surface to the center of the joint where the detector was placed was measured (by digital caliper) to be 2.4 cm. From the curve in Figure 3, and assuming this dog to be a simple tank of water, we would predict the beam to transmit about 50% of its intensity to this depth. From an MRI-Monte Carlo simulation of this anatomical configuration, and including the estimated attenuation of skin, bone, fat, muscle, and joint tendons, we predict transmission of something more like only 5%. From the Si photodiode measurement, we find that only about 2% of the beam is transmitted to the center of the joint.

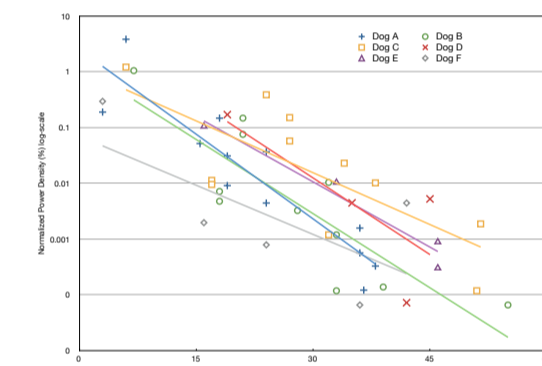


Figure 5: Generalized Penetration Data for Eight Canine Cadaver Legs

DISCUSSION and CONCLUSIONS

As expected, the first-order experiments under-estimated the beam attenuation, but Monte Carlo results served as an accurate prediction of *ex vivo* observation. Dose delivered at therapeutic depths are up to 2 and 3 orders of magnitude less than those delivered to the surface. With enough data using a variety of skin, tissue, and bone thicknesses, this type of analysis will yield a full dosimetric profile.

Much more work remains to be done in quantitative internal dosimetry of laser therapy. This study, however, is a necessary step in the right direction on the path of understanding the orders of magnitude involved. Once further enlightened, we will be able to review both existing and future studies to better understand the biological effect of the delivered dose that came from the reported treatment prescriptions, and eventually converge on the optimal treatment parameters for clinical success.

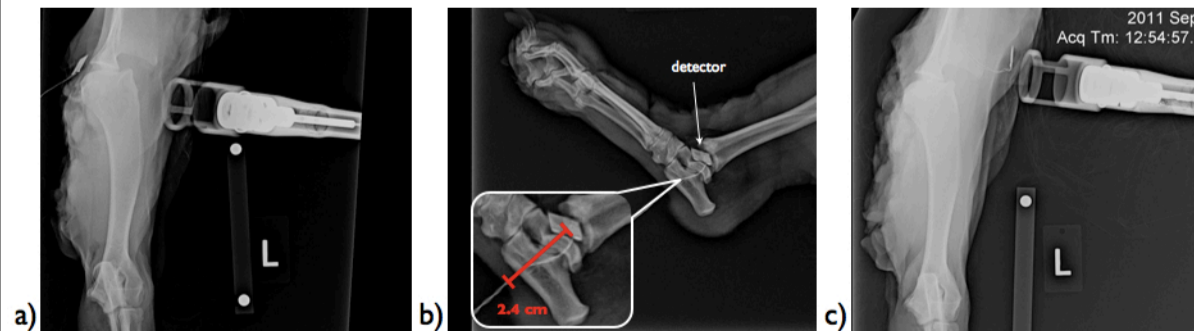


Figure 6: Radiograph Examples of Anatomical Orientation of Detectors in Cadavers

REFERENCES

- [1] W. Cheong, S.A. Prael, and A.J. Welch. A Review of the Optical Properties of Biological Tissue. *IEEE Journal of Quantum Electronics*, 26(12):2166–2185, 1990.
- [2] Q. Fang and D.A. Boas. Monte Carlo simulation of photon migration in 3d turbid media accelerated by graphics processing units. *Optics Express*, 17(22):20178–20190, 2009.
- [3] S.J. Matcher, M. Cope, and D.T. Delpy. *In vivo* measurement of the wavelength dependence of tissue-scattering coefficients between 760 and 900 nm measured with time-resolved spectroscopy. *Applied Optics*, 36(1):386–396, 1997.
- [4] C.R. Simpson, M. Kohl, M. Essenpreis, and M. Cope. Near-infrared optical properties of *ex vivo* human skin and subcutaneous tissues measured using the Monte Carlo inversion technique. *Phys. Med. Biol.*, 43:2465–2478, 1998.